HHS Public Access

Author manuscript

Mater Sci Eng C Mater Biol Appl. Author manuscript; available in PMC 2019 October 01.

Published in final edited form as:

Mater Sci Eng C Mater Biol Appl. 2018 October 01; 91: 330–339. doi:10.1016/j.msec.2018.05.060.

Comparative investigation of porous nano-hydroxyapaptite/chitosan, nano-zirconia/chitosan and novel nano-calcium zirconate/chitosan composite scaffolds for their potential applications in bone regeneration

Bipin Gaihre[1] and **A. Champa Jayasuriya**[1,2,*]

[1]Department of Bioengineering, The University of Toledo, Toledo, OH 43614, USA

[2]Department of Orthopaedic Surgery, University of Toledo Medical Center, Toledo, OH 43614, USA

Abstract

Zirconium (Zr) based bioceramic nanoparticles, as the filler material to chitosan (CS), for the development of composite scaffolds are less studied compared to hydroxyapatite nanoparticles. This is predominantly due to the biological similarity of nano-hydroxyapatite (nHA; $Ca_{10}(PO_4)_6(OH)_2$) with bone inorganic component. In this study, we compared the physical and biological properties of CS composite scaffolds hybridized with nHA, nano-zirconia (**nZrO; ZrO_2**), and nano-calcium zirconate (**nCZ; $CaZrO_3$**). For the first time in this study, the properties of CS-nCZ composite scaffolds have been reported. The porous composite scaffolds were developed using the freeze-drying technique. The compressive strength and modulus were in the range of 50–55 KPa and 0.75–0.95 MPa for composite scaffolds, significantly higher ($p<0.05$), compared to CS alone scaffolds (28 KPa and 0.25 MPa) and were comparable among CS-nHA, CS-nZrO, and CS-nCZ scaffolds. Peak force quantitative nanomechanical mapping (PFQNM) using an atomic force microscope (AFM) showed that the Young's modulus of composite material was higher compared to only CS ($p<0.001$), and the values were similar among the composite materials. One of the major issues in the use of Zr based bioceramic materials in bone tissue regeneration applications is their lower osteoblasts response. This study has shown that CS-nCZ supported higher proliferation of pre-osteoblasts compared to CS-nZrO and the spreading was more similar to that observed in CS-nHA scaffolds. Taken together, results show that the physical and biological properties, studied here, of CS composite with Zr based bio-ceramic was comparable with CS-nHA composite scaffolds and hence show the prospective of CS-nCZ for future bone tissue engineering applications.

Graphical abstract

*Corresponding author. Department of Orthopaedic Surgery, University of Toledo Medical Center, 3000 Arlington Avenue, Toledo, OH 43614, USA, Tel: +1-429-383-6557, Fax: +1-419-383-3526, a.jayasuriya@utoledo.edu.

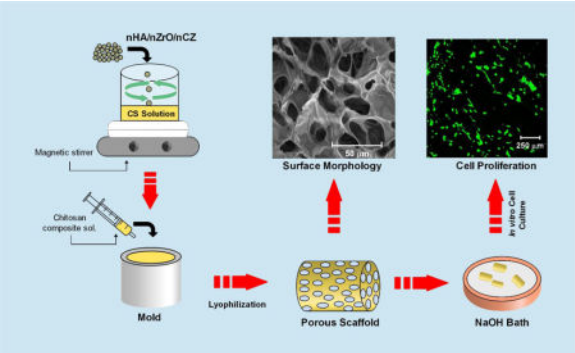

Keywords

Chitosan; Composite; Nano-bioceramics; Mechanical properties; Atomic force microscopy; Cell proliferation

1. Introduction

Bone tissue engineering approaches have been adapted as a promising tool to reconstruct and restore the functionality of defective and lost bone [1–3]. Scaffolds developed to be applied for this application are required to have good mechanical strength to support new bone formation and cytocompatibility properties to enable cell proliferation in addition to their three-dimensional (3-D) interconnected porous networks that allow cell migration and nutrient transport [4, 5].

Various materials have been used to develop the bone scaffolds including polymers, ceramics, metals and composites [4]. Natural bone matrix is a composite consisting of organic (25%) and inorganic (65%) components. Collagen I constitutes as the major portion of organic component, and hydroxyapatite constitutes as the inorganic component of bone [6]. The composite scaffolds forming a hybrid of organic and inorganic biomaterials are thus considered an attractive option to mimic the natural bone composition [7–9]. Composite scaffolds developed from chitosan (CS) and hydroxyapatite (HA) have been selected extensively because of their biocompatibility, and osteoconductive properties [8, 10]. *HA constitutes the major inorganic component of bone and thus has been extensively used to prepare the bone scaffolds. Recent studies have shown that the morphology of HA could be modified to develop the composite scaffolds with improved mechanical and biological properties. It has been used as nano-powder, nano wires, microspheres, and microtubes with CS to develop the composites with improved mechanical and drug delivery properties* [11, 12]. CS is one of the highly-used polysaccharide based biopolymers used to develop composites because of its suitable chemical structure, biocompatibility and biodegradability. CS only scaffolds cannot imitate all the properties of natural bone as they are flexible with lower mechanical strength and are not osteoconductive itself. The addition of HA into CS, however, adds to the mechanical strength and improves the osteogenic property of the composites [13–15]. The brittle nature, low tensile and fracture strength of HA, sometime limits its use in the composite scaffolds [16]. In a quest to find a comparable and better filler material than HA, we compared the physical and biological properties of zirconia (ZrO) and

calcium zirconate (CZ) nano-powder addition to develop CS-nZrO and novel CS-nCZ composite scaffolds.

ZrO is a ceramic biomaterial with good biocompatibility and high fracture strength. It has been reported to significantly improve the mechanical properties of other ceramic materials such as calcium phosphate, HA, and bioglass [17–19]. The presence of zirconium has been shown to improve the *in vitro* osteoblasts response [20, 21]. nZrO has been used as filler material into polymeric scaffolds and shown to improve their mechanical and swelling properties without causing any cytotoxic effects to the pre-osteoblasts [22–24]. Few studies have reported the attenuation of cell adhesion and proliferation on ZrO rich scaffolds due to the low affinity of ZrO to the proteins [18, 25]. Taking these into consideration, CZ was studied as a potential zirconium based bio-ceramics for its usability as a filler material into CS scaffolds. CZ is calcium oxide (CaO) stabilized ZrO that is mostly used as a solid electrolyte to develop electrochemical oxygen sensors due to its high oxygen conductivity [26]. CZ phase was observed when ZrO was sintered with HA at 1500 °C that imparted HA-ZrO composites with high mechanical strength [18]. Studies have shown that calcium released from the bio-cements can mediate the expression of osteopontin which can provide the integrin binding domain, and hence, promoting the cell attachment and proliferation [27, 28]. We believe that presence of calcium in CZ promotes the protein adsorption and thus improve the cell adhesion and proliferation while also providing the sufficient mechanical strength to the CS scaffolds.

In this study, we compared the physical and biological properties of CS scaffolds and its composites with nHA, nZrO and nCZ. To our knowledge, CS-nCZ composite scaffold properties have been reported for the first time in this study. The scaffolds were fabricated using conventional freeze-drying technique to obtain the porous structure and were compared in terms of morphology, mechanical properties, swelling characteristics as well as cell attachment and proliferation. In order to gain the insight into nano-mechanical properties of nano-composite scaffold materials, atomic force microscopy was used for comparative analysis of Young's modulus.

2. Materials and methods

2.1 Materials

Medium molecular weight chitosan (75–85% degree of deacetylation), acetic acid, and the bio-ceramics nanopowder including hydroxyapatite (<200nm), zirconium oxide (<100nm), and calcium zirconate (<50nm) were all purchased from Sigma-Aldrich (USA). Sodium hydroxide (NaOH) and the cell culture medium components including alpha-minimum essential media (α-MEM, Gibco), fetal bovine serum (FBS), and penicillin/streptomycin were all supplied by ThermoFisher Scientific (USA). Deionized ultrapure water was used throughout the experiments.

2.2 Scaffolds preparation

2.5% CS solution was prepared by dissolving the CS powder in 2% acetic acid using magnetic stirrer and filtered through the nylon mesh with the pore size of 50 μm to remove

the insoluble components. The bio-ceramics nanopowder was then added to filtered CS solution at 40% (w/w) and vigorously stirred at 40 °C. In order to ensure the homogenous dispersion of nanopowder on CS solution, it was repetitively stirred and sonicated at 40°C. The CS composite solution was then loaded into a syringe and degassed to remove the air-bubbles formed due to vigorous stirring. The material was then injected into the cylindrical molds with the approximate dimensions of diameter (d) =6 mm and length (l) =12 mm for compressive testing (figure 1). The molds were placed between two glass slides, transferred to −80°C for 12 h, and allowed to lyophilize for 24 h in a freeze dryer (Labconco Freezone 4.5L, Kansas, MO, USA). The composite scaffolds, thus obtained, were stored in an air tight container before further characterization. The excess acetic acid on the scaffolds was neutralized by immersing them in the 0.5 N NaOH bath and washing with water DI water. For cell culture experiments the neutralized scaffold was lyophilized again in a freeze dryer for 24 h.

2.3 Morphology of scaffolds and elemental analysis

The morphology of prepared scaffolds was examined by Scanning electron microscope (SEM) and *the energy dispersive X-ray spectroscopy (EDX) was used for the elemental mapping along the surface (Quanta, FEI, Holland). Elemental mapping was performed only for the composite scaffolds to observe the distribution of nanoparticles along their surface. Calcium (Ca) and phosphate (P) was mapped for CS-nHA scaffolds, zirconium (Zr) and oxygen (O) was mapped for CS-nZrO scaffolds and Zr and Ca was mapped for CS-nCZ scaffolds.* 2 mm thick sliced scaffolds were each loaded onto an aluminum stub using double sided carbon tape and sputter coated with gold/palladium (Cressington Scientific Instruments, UK) for 40 s before imaging them under SEM. The operating voltage for the imaging was 20 kV, and the images were taken at different magnifications to observe the porous morphology as well as the surface of scaffold walls. *For the elemental mapping using EDX, the SEM images captured were transferred into the INCA software for elemental mapping. The mapping was started after the signal counts reached more than 10000 for all the composite scaffolds.*

2.4 Physical structure of scaffolds-X-ray diffraction (XRD)

The phase analysis of the materials in the composite scaffold was performed using XRD n (Rigaku Ultima III, Japan) in a focused beam mode. The scaffold was grinded into fine powders and loaded into aluminum sample holder for the analysis. The working condition of the diffractometer was Cu Kα radiation with a rotating anode at 40 kV and 44 mA. The data was collected in the step width 0.05 with scattering angle (2Θ) ranging from 10° to 80°.

2.5 Water absorption properties and porosity measurement

The water absorption capacity was determined after 24 h and 48 h by immersing the neutralized scaffolds in 1X PBS at 37°C. Before immersing them in PBS, dry weight (W_d) of the scaffolds was measured and recorded. The immersed scaffolds after specified time were dried superficially using filter paper, and the wet weight (W_w) was measured. Each study was performed in triplicates, and the average value was taken. The equilibrium water absorption (W_A) was calculated as:

$$W_A(\%) = \frac{(W_A - W_d)}{W_d} \times 100 \quad (1)$$

The porosity of the scaffolds was evaluated by using liquid displacement method [29]. The dry weight of the scaffolds was recorded first (W_d) followed by the immersion in ethanol for 24 h until saturation. The wet weight (W_w) of the scaffolds was measured after taking out the scaffolds from the ethanol. The porosity was calculated as:

$$\text{Porosity}(\%) = \frac{(W_w - W_d)}{\rho \times V} \times 100 \quad (2)$$

ρ refers to the density of the ethanol and **V** refers to the initial volume of the scaffolds.

2.6 Mechanical properties

2.6.1 Compressive strength—The compressive strength of as-prepared scaffolds was measured using MTESTQuattro Universal Testing Machine (Admet, USA) fitted with 1 kN load cell at room temperature. Cylindrical scaffolds with the diameter of 6 mm and length of 12 mm were compressed at the crosshead speed of 0.6 mm/min until the length of the sample was reduced by 50%. Seven samples from each group were tested, and the obtained load-displacement data was converted into stress-strain curve to find the compressive strength and modulus. The yield point on compression was determined by 0.2% offset in strain value. The stress at this point and the slope of the linear portion of the curve is reported as compressive stress and compressive modulus.

2.6.2 Nano mechanical properties

2.6.2.1 Background theory: Atomic Force Microscopy (AFM) (Bruker Multimode) in PeakForce Quantitative Nanomechanical Mapping (PFQNM) mode was used to determine the nano mechanical property of the scaffold materials. The operation in this mode facilitates the generation of force curves that can be used to extract quantitative mechanical data such as Young's modulus. The modulus is calculated using the Derjaguin, Mullerm, Toropov (DMT) model which is a modified Hertzian model that uses the linear part of retract curve (Fig 2) and takes adhesive force between tip and the sample into account [30].

The reduced Young's modulus per this model is given by

$$E_r = \frac{3(F_{tip} - F_{adh})}{4\sqrt{(Rd^3)}} \quad (3)$$

In the above equation, F_{tip} is the force on the AFM tip, F_{adh} is the adhesive force between the tip and the sample, R is the tip radius, and d is the deformation depth.

Poisson's ratio converts the measured reduced Young's modulus into sample Young's modulus E_s given by

$$\frac{1}{E_r} = \frac{(1 - \nu_s^2)}{E_s} + \frac{(1 - \nu_t^2)}{E_t} \quad (4)$$

where υ_t and E_t are the Poisson's ratio and Young's modulus of tip, υ_s and E_s are the Poisson's ratio and Young's modulus of sample. The assumption here is that the tip modulus is much higher than sample modulus, E_s, and hence can be considered infinite and thus the sample modulus is calculated using sample's Poisson's ratio.

2.6.2.2 AFM Measurement: The chitosan composite solution with homogenously dispersed bioceramics powder was cast into a glass substrate purified with ethanol. The cast scaffolds were dried overnight at room temperature and stored in a vacuum desiccator before performing the test. The measurements were performed using Bruker Multimode 8 AFM fitted with J-scanner. RTESPA-525 probe with rectangular cantilever made from antimony doped silicon and with the spring constant of 200 N/m was used. This probe was selected based on the recommendation of Bruker for the range of Young's moduli reported for CS. NanoScope software was used to set the parameters for measurement and NanoScope Analysis was used to find the Young's modulus from the collected modulus data. The quantitative nano mechanical data was obtained after performing the absolute calibration of the probe parameters (deflection sensitivity and tip radius). Each sample was scanned over an area of 1.5 μm × 1.5 μm at the scan rate of 0.5 Hz at three different locations. Five samples from each group was measured and thus the modulus value reported is an average of 15 measurements for each group of samples. Polystyrene standard sample of known Young's modulus was scanned before measuring each sample to ensure that tip was not wearing out.

2.7 Cell culture and seeding on scaffolds

Cell culture studies were performed using mouse pre-osteoblast cells (OB-6). Alpha minimum essential medium supplemented with 15% FBS and 1% penicillin-streptomycin was used to culture pre-osteoblasts. Prior to the cell seeding, the neutralized cylindrical scaffolds of 2 mm thickness were placed in 24-well plates for UV-sterilization inside cell culture hood for 45 mins. The sterilized samples were incubated with culture medium for 5 h at 37°C and 5% CO_2. Swelled scaffolds were then transferred into different wells and 200 μl of cell suspension containing 50,000 to 10^5 cells was added to the top of the scaffolds slowly allowing cells to distribute throughout the scaffolds. The cell-seeded scaffolds afterward were incubated at 37°C and 5% CO_2 for 3 h to allow the cells to attach to the scaffold. An additional 800 μl of culture medium was added after 3 h, and the incubation was resumed. This seeding technique was adopted as most of the scaffolds seemed to be floating on the culture medium due to high porosity. The culture medium was replaced every 3 days through the duration of this study.

2.8 Cell viability and proliferation on scaffolds

The proliferation of pre-osteoblasts, along the surface and into the scaffold, was observed using confocal laser scanning microscope (CLSM) (Leica, USA) after staining the cells with calcein AM. The cell-scaffold constructs, at day 10 and 20, were transferred into new wells and washed with 1X PBS twice. The calcein AM dye in 1X DBPS was then added to the wells and incubated at 37°C for 15 min. The viable cells proliferating on the scaffold were observed as green fluorescence produced from calcein at 488 nm enzymatically converted from calcein AM by the viable cells. The images were collected at the depth of 200 μm from the surface with the step size of 10 μm. The images thus collected as Z-slices were processed for 3-D projection to obtain the reconstructed images.

2.9 Cell morphology on scaffolds

SEM can be considered as a suitable technique to observe the spreading pattern and morphology of cells on the scaffold. The scaffolds seeded with 10^5 cells, at day 7 and 14, were transferred into new wells and washed with 1X PBS twice. The fixation of cells into the scaffold was done by immersing cell-scaffold constructs into 2.5% glutaraldehyde in a cacodylate buffer (pH 7.4) and incubating at 4°C for 1 h. After washing with 1X PBS, they were dehydrated by immersing in a series of ethanol dilution (30%, 50%, 70%, and 90%), three times each for 3 min, and finally in 100% ethanol, two times each for 5 min. Lastly, they were immersed in 100% HDMS and kept inside a hood overnight for complete drying. The dried cell-scaffold constructs were then sputter coated with gold for 45 min and imaged using SEM at 20 kV.

2.10 Statistical analysis

Experimental data are presented as mean ± standard deviation. The statistical difference between the groups was determined using one way ANOVA followed by Tukey's post hoc analysis. P-value of less than 0.05 was considered as statistically different.

3.0 Results and discussion

3.1 SEM-EDX analysis

The scaffolds to be used in tissue engineering application should have a porous structure with open and well interconnected pores. In addition to openness and interconnectivity, the size of the pores affects the attachment, proliferation and differentiation of cells [31]. The microstructure of CS only and composite scaffolds presented in figure 3 shows a highly porous structure with good interpore connectivity. The macroscopic morphology of all the scaffolds was similar with distributed pores along the surface. The porous structure looked more uniform and less distorted on the composite scaffolds compared to CS only scaffolds that exhibited irregular and undefined contour. The quantitative analysis of pore size of several images using ImageJ showed the pore size of 10–50 μm for CS only scaffolds and 25–100 μm for composite scaffolds. A greater range of pore sizes was observed on the composite scaffolds which could be beneficial as the studies have shown that the small pore size ensures the mechanical integrity whereas the large pore size facilitates the cell migration and nutrient transport [32, 33]. The pores of CS-nCZ scaffold appeared well defined and

uniform in shape and the average pore size of CS-nZrO and CS-nCZ scaffolds was higher than CS-nHA scaffolds. This could be due to the reported smaller size and higher surface area of nZrO (<100 nm and 25 m^2/g) and nCZ (<50 nm and 55–65 m^2/g) compared to nHA (<200 nm and 9.4 m^2/g). The transmission electron microscopy (TEM) images for the nanoparticles (supplementary material) showed that the average size of nZrO was 27.34 nm with the size ranging from 22 to 50 nm, nCZ was 15.91 nm with the size ranging from 7 to 25 nm, and nHA was 52.45 nm with the size ranging from 30 to 90 nm. This might have resulted in the better dispersion and distribution of nZrO and nCZ on CS than that of nHA. The images taken at high magnification showing microscopic morphology of scaffold wall are presented in figure 3 (B, D, F, H). The CS only scaffolds had a relatively smooth surface compared to composite scaffolds, where the pore walls were rougher due to the presence of bio-ceramics nanoparticles.

The elemental mapping representative images for the composite scaffolds on figure 4 show the distribution of nanoparticles along the porous surface. It can be observed that the no bigger clumps or agglomeration of particles around the porous surface was observed for all of the composite scaffolds. The nanoparticles looked to be uniformly distributed along the porous surface as demonstrated by the uniformity in the distribution of elemental components of nanoparticle.

3.2 XRD analysis

XRD analysis was done to analyze the phase of bio-ceramic on composite scaffolds. The characteristic diffraction pattern for materials used is shown in figure 5. XRD pattern of CS shows a peak at $2\Theta = 20°$, which is the characteristic XRD peak of CS. The major peaks for nHA observed at 25.8°, 28.8°, 31.7°, 32.8°, 46.6°, and 49.35° correspond to 002, 210, 211, 112, 312, and 213 miller indices, respectively [34]. These peaks were present in the XRD pattern of CS-nHA composite scaffolds in addition to the characteristic peak of CS at 20° which was broader and less intense than in the XRD pattern of only CS. The crystalline phase of ZrO depends on the temperature at which it is synthesized. Monoclinic phase is more prevalent at lower temperatures (<1100 °C), tetragonal phase at intermediate, and cubic at higher temperatures (>2300 °C). nZrO obtained commercially is a pure monoclinic ZrO. XRD pattern of nZrO shows its monoclinic phase specific peaks at 24.2°, 28.3°, 31.5°, 34.4°, 35.4°, and 51.3° corresponding to the 110, −111, 111, 002, 200, and 220 planes, respectively [35]. Most of these peaks were observed in CS-nZrO composite, indicating the crystallinity of nZrO was not affected, but the characteristic peak of CS disappeared. Similarly, the XRD pattern of bulk nCZ is also presented in figure 5. The characteristic peak for nCZ present at 22.2°, 31.5°, 45.2°, 50.9°, 55.6°, and 56.8° corresponds to 101, 121, 202, 222, 042, and 123 planes, respectively [36].

3.2 Water absorption study and porosity measurement

The absorption of water by the scaffolds enable the cell infiltration and increase the probability of cell growth in a three-dimensional structure. In addition, high degree of swelling also enhances the ability of scaffolds to absorb the nutrients from culture medium [37]. Water uptake experiment was performed to study the influence of bioceramics nano-powder addition on the absorption of physiological fluid by the scaffolds. As shown in

figure 6, significantly high degree of swelling was observed on CS only scaffolds compared to CS-nHA scaffolds after 24 h, and all composite scaffolds after 48 h indicating that the addition of bio-ceramics nano powder to pure CS decreases the degree of water absorption. The swelling ratio remained same for CS only scaffolds after 24 h and 48 h (911.6 ± 37.56% and 912.8 ± 22.12% respectively). *The swelling ratio for composite scaffolds, however, was slightly lower at 48 h compared to that at 24 h of immersion in PBS (not significant). This might be due to the slight release of bio-ceramics nanoparticles from the scaffolds into the PBS as a result of which the wet weight of the scaffolds reduced after 48 h.* Although, the water absorption capacity of composite scaffolds was lower than CS alone scaffolds, it was high enough to ensure the cell infiltration and nutrient transportation and are expected to hold higher mechanical strength. CS-nZrO scaffolds, among the composites, had slightly higher water absorption compared to CS-nHA and CS-nCZ scaffolds, at both time points. This could be due to the presence of hygroscopic metal oxide surface of nZrO that increased the water absorption capacity of CS-nZrO as well as possible interaction of calcium and phosphate in nHA and calcium in nCZ to OH and NH_2 groups in CS that decreased the water absorption capacity of CS-nHA and CS-nCZ scaffolds [22, 37].

The porosity percent of the scaffolds was measured using liquid displacement method using ethanol. The porosity measurement showed that the scaffolds were highly porous with value ranging from 85% to 94% depending on the composition. The porosity of CS only (94.5 ± 3.8%) and CS-nCZ (94.1 ± 13.3%) was higher compared to the CS-nHA (87.5 ± 11.2%) and CS-nZrO (85.2 ± 9.76%). The porosity of these scaffolds can be considered high enough to allow the transportation of nutrients as well as cellular ingrowth which is important for the regeneration of a complete tissue.

3.3 Mechanical properties

The major constraint of using natural polymer based scaffolds, such as CS, in bone regeneration applications is their lower mechanical strength. One of the extremely used approaches to overcome it is to incorporate bio-ceramic nanoparticles into the polymer matrix [8]. CS has been extensively studied as composite scaffolds with nHA whereas there are very less studies on CS-nZrO and no study on CS-nCZ composites. In this study, we compared the compressive strength and modulus of these composite scaffolds. In addition, we also compared the nano mechanical strength of these composites to get a better insight into their mechanical properties.

3.3.1 Compressive test—The compressive strength and compressive modulus of the scaffolds are shown in figure 7. The visual inspection of the scaffolds showed that the composite scaffolds were stiffer and easier to handle than CS only scaffolds which were softer and weaker. The measurement data showed that the compressive strength of the composite scaffolds was higher than the pure CS scaffolds. The compressive strength of all the composite scaffolds was comparable. The compressive modulus, determined from linear region of stress-strain curve, was about 0.24 MPa for CS only scaffolds whereas it was about 0.76 MPa, 0.774 MPa and 0.97 MPa for CS-nHA, CS-nZrO and CS-nCZ scaffolds respectively. The comparison of the strength values among the composite scaffolds showed that when added at equal weight ratio to CS, nZrO and nCZ had comparable strength and

modulus to nHA and even better compressive modulus was obtained for nCZ compared to all other groups.

3.3.2 Nano-mechanical property—The local nano-mechanical properties of a scaffold play an important role in cell differentiation and tissue regeneration functions [38]. Due to the high porosity, it was difficult to obtain nano-mechanical property data from the scaffolds. A comparative analysis for nano-mechanical property was thus done by casting the CS composite solution onto a glass slide for measurement. The results presented on figure 8, show that the addition of bio-ceramics nano-powder significantly improved the Young's modulus of CS. There was no statistical difference in Young's modulus among the different composite groups, but the results show higher values for the CS-nCZ group compared to other composite groups. This comparative study shows that nZrO and nCZ can behave similarly or even better, in terms of nano-mechanical property, compared to nHA particles, when added to CS.

Zirconia is a high strength bioceramics reported to have a high toughness and Young's modulus compared to some metals such as stainless steel. Zirconia-hydroxyapatite composites are reported to have a higher mechanical strength than hydroxyapatite [18]. This study, however, showed that simple mixing and dispersion of zirconia based bio-ceramics nanoparticles on CS is not sufficient to produce significantly higher bulk and nano-mechanical strength than nHA, though they were comparable.

3.4 Cell proliferation study

Biomaterials intended to be applied in tissue engineering application should not cause any toxic effect to the cells. CS is reported to be non-toxic to the osteoblasts and the incorporation of nHA into CS improves its osteogenic property [10]. The proliferation of pre-osteoblasts along the surface and into the porous structure of scaffolds was investigated using CLSM after staining the cells with calcein AM. Calcein AM is a cell-permeant dye that gives green fluorescence when converted into calcein by the viable cells. The images shown in figure 9 are reconstructed from the slices of 10 μm thickness along the Z-depth of 300 μm into the scaffold. This Z-volume was chosen based on the observation of penetration of cells into the scaffold. The cells growing on all the scaffolds on day 14 was higher in number, indicated by the green fluorescence, than on day 7. The images also show that the proliferation of cells at both time points was higher on composite scaffolds than on the CS only scaffolds. Particularly, the proliferation of cells was much better on CS-nHA and CS-nCZ scaffolds (Fig 9 B, F, D, and H), compared to other groups.

ZrO has been reported to be bio-inert, and thus a bioactive coating was applied to improve its interaction with cells and tissues [39]. Few studies have reported the use of nZrO filler into polymer matrix as a scaffold with improved bio-mineralization, protein absorption, and osteogenic properties [23]. In this study, we observed the similar results as the cell proliferation on CS-nZrO looked better than on CS only scaffolds. The proliferation of cells on CS-nHA and CS-nCZ was better than that on CS-nZrO. This could be due to the presence of calcium on nHA and nCZ. Studies have shown that the increase in extracellular calcium plays a critical role in osteoblast proliferation. The increased level of extracellular calcium

induces the chemotaxis and proliferation of osteoblasts, induced by the calcium sensing receptors. CS-nCZ would be more advantageous in this respect, as nCZ possesses the properties of Zr based ceramics (mechanical strength) and can promote the osteoblasts growth and proliferation due to the presence of calcium.

3.5 Morphology of cells

The morphology of cells attached and proliferating on the surface of the scaffolds at day 7 and 14 was observed using SEM (Figure 10). At day 7, a strong cellular adhesion and growth at low density were observed on CS-nHA and CS-nCZ scaffolds with extensive filopodia, flat morphology, and excellent spreading. The cells were less flattened and had more circular morphology on CS and CS-nZrO scaffolds. More interestingly, on all composite scaffolds, the cells were in close contact with the scaffold surface and extending their filopodia more toward the nano bio-ceramics particles incorporated into scaffold (shown by arrows on figure 10), thus showing the importance of these nanoparticles in cell attachment and spreading. The greater osteoblasts spreading on the surface of scaffold can result in better cell proliferation and differentiation. The presence of calcium in nHA has been found to increase its binding affinity to the serum protein, osteocalcin, and increase the expression and synthesis of osteopontin. Osteopontin contains Arg-Gly-Asp oligopeptide, a cell binding site for cell integrin receptors [27, 28]. This might have favored the spreading of cells onto CS-nHA and possibly CS-nCZ scaffold due to presence of calcium in nCZ.

At day 14, an increased cell density with better cell to cell contact and sheet like morphology was observed and was found to be more prominent on composite scaffolds compared to CS only scaffolds. The cells in CS-nHA grew in big colonies and were clearly visible due to the more defined shape of the cells in colonies. The cells in CS-nZrO and CS-nCZ were forming a sheet along the surface of the scaffold and especially in CS-nCZ, cells were not clearly visible as they were covering the whole scaffold surface in a sheet form.

4. Conclusion

In this study, we performed the comparative investigation of physical and biological properties of CS-nHA, CS-nZrO, and a novel CS-nCZ composite scaffolds intended for bone regeneration applications. The addition of bio-ceramics nanopowder into CS scaffolds greatly improved their overall properties including mechanical strength, cell proliferation, and cell spreading on the scaffolds. The scaffolds have sufficient water absorption capacities and porosities. The compressive strength was higher for CS-nZrO and CS-nCZ, and compressive modulus was higher for CS-nCZ compared to CS-nHA. Though the result was not significant, it shows the prospective of zirconium based bio-ceramics to be used with CS for development of bone composite scaffolds. AFM results showed that the Young’s modulus of all the composites was similar, but was significantly higher than pure CS. The attachment and proliferation of pre-osteoblasts looked much better with extended filopodia on CS-nHA and CS-nCZ compared to CS-nZrO composite scaffolds. Extended studies on the osteogenic potential of CS-nCZ will be conducted in the near future. Taken together, this study shows the potential of CS-nZrO and novel CS-nCZ composite scaffolds for bone regeneration applications.

Acknowledgments

We would like to acknowledge National Institute of Health (NIH) grant number R01DE023356 for support. This work would not have been possible without their financial support. We would also like to thank Mr. Israel Okeke for his help to prepare the figures.

References

1. Henkel J, Woodruff MA, Epari DR, Steck R, Glatt V, Dickinson IC, Choong PFM, Schuetz MA, Hutmacher DW. Bone Regeneration Based on Tissue Engineering Conceptions — A 21st Century Perspective. Bone Research. 2013; 1(3):216–248. [PubMed: 26273505]
2. Dimitriou R, Jones E, McGonagle D, Giannoudis PV. Bone regeneration: current concepts and future directions. BMC Medicine. 2011; 9(1):66. [PubMed: 21627784]
3. Black CRM, Goriainov V, Gibbs D, Kanczler J, Tare RS, Oreffo ROC. Bone Tissue Engineering. Current Molecular Biology Reports. 2015; 1(3):132–140. [PubMed: 26618105]
4. Polo-Corrales L, Latorre-Esteves M, Ramirez-Vick JE. Scaffold Design for Bone Regeneration. Journal of nanoscience and nanotechnology. 2014; 14(1):15–56. [PubMed: 24730250]
5. Stevens MM. Biomaterials for bone tissue engineering. Materials Today. 2008; 11(5):18–25.
6. Feng X. Chemical and Biochemical Basis of Cell-Bone Matrix Interaction in Health and Disease. Current chemical biology. 2009; 3(2):189–196. [PubMed: 20161446]
7. Yi H, Ur Rehman F, Zhao C, Liu B, He N. Recent advances in nano scaffolds for bone repair. Bone Research. 2016; 4:16050. [PubMed: 28018707]
8. Deepthi S, Venkatesan J, Kim SK, Bumgardner JD, Jayakumar R. An overview of chitin or chitosan/nano ceramic composite scaffolds for bone tissue engineering. International Journal of Biological Macromolecules. 2016; 93(Part B):1338–1353. [PubMed: 27012892]
9. Gaihre B, Lecka-Czernik B, Jayasuriya AC. Injectable nanosilica–chitosan microparticles for bone regeneration applications. Journal of biomaterials applications. 2018; 32(6):813–825. [PubMed: 29160129]
10. Thein-Han WW, Misra RDK. Biomimetic chitosan–nanohydroxyapatite composite scaffolds for bone tissue engineering. Acta Biomaterialia. 2009; 5(4):1182–1197. [PubMed: 19121983]
11. Sun TW, Zhu YJ, Chen F. Highly Flexible Multifunctional Biopaper Comprising Chitosan Reinforced by Ultralong Hydroxyapatite Nanowires. Chemistry – A European Journal. 2016; 23(16):3850–3862.
12. Zhang YG, Zhu YJ, Chen F, Sun TW. A novel composite scaffold comprising ultralong hydroxyapatite microtubes and chitosan: preparation and application in drug delivery. Journal of Materials Chemistry B. 2017; 5(21):3898–3906.
13. Kong L, Gao Y, Lu G, Gong Y, Zhao N, Zhang X. A study on the bioactivity of chitosan/nano-hydroxyapatite composite scaffolds for bone tissue engineering. European Polymer Journal. 2006; 42(12):3171–3179.
14. Cai X, Tong H, Shen X, Chen W, Yan J, Hu J. Preparation and characterization of homogeneous chitosan–polylactic acid/hydroxyapatite nanocomposite for bone tissue engineering and evaluation of its mechanical properties. Acta Biomaterialia. 2009; 5(7):2693–2703. [PubMed: 19359225]
15. Gaihre B, Uswatta S, Jayasuriya AC. Nano-scale characterization of nano-hydroxyapatite incorporated chitosan particles for bone repair. Colloids and Surfaces B: Biointerfaces. 2018; 165:158–164. [PubMed: 29477936]
16. Wang H. Hydroxyapatite degradation and biocompatibility. 2004
17. Afzal A. Implantable zirconia bioceramics for bone repair and replacement: A chronological review. Materials Express. 2014; 4(1):1–12.
18. An SH, Matsumoto T, Miyajima H, Nakahira A, Kim KH, Imazato S. Porous zirconia/hydroxyapatite scaffolds for bone reconstruction. Dental Materials. 2012; 28(12):1221–1231. [PubMed: 23018082]
19. Ruiz-Aguilar C, Aguilar-Reyes EA, Flores-Martínez M, León-Patiño CA, Nuñéz-Anita RE. Synthesis and characterisation of β-TCP/bioglass/zirconia scaffolds. Advances in Applied Ceramics. 2017; 116(8):452–461.

20. Chen Y, Roohani-Esfahani SI, Lu Z, Zreiqat H, Dunstan CR. Zirconium Ions Up-Regulate the BMP/SMAD Signaling Pathway and Promote the Proliferation and Differentiation of Human Osteoblasts. PLOS ONE. 2015; 10(1):e0113426. [PubMed: 25602473]
21. Gaihre B, Jayasuriya AC. Fabrication and characterization of carboxymethyl cellulose novel microparticles for bone tissue engineering. Materials Science and Engineering: C. 2016; 69:733–743. [PubMed: 27612767]
22. Bhowmick A, Pramanik N, Jana P, Mitra T, Gnanamani A, Das M, Kundu PP. Development of bone-like zirconium oxide nanoceramic modified chitosan based porous nanocomposites for biomedical application. Int J Biol Macromol. 2017; 95:348–356. [PubMed: 27865958]
23. Teimouri A, Ebrahimi R, Emadi R, Beni BH, Chermahini AN. Nano-composite of silk fibroin–chitosan/Nano ZrO2 for tissue engineering applications: Fabrication and morphology. International Journal of Biological Macromolecules. 2015; 76:292–302. [PubMed: 25709014]
24. Bhowmick A, Pramanik N, Mitra T, Gnanamani A, Das M, Kundu PP. Mechanical and biological investigations of chitosan-polyvinyl alcohol based ZrO2 doped porous hybrid composites for bone tissue engineering applications. New Journal of Chemistry. 2017; 41(15):7524–7530.
25. Malmström J, Adolfsson E, Emanuelsson L, Thomsen P. Bone ingrowth in zirconia and hydroxyapatite scaffolds with identical macroporosity. Journal of Materials Science: Materials in Medicine. 2008; 19(9):2983–2992. [PubMed: 17483890]
26. Róg G, Dudek M, Kozłowska-Róg A, Bućko M. Calcium zirconate: preparation, properties and application to the solid oxide galvanic cells. Electrochimica Acta. 2002; 47(28):4523–4529.
27. Ros-Tárraga P, Rabadan-Ros R, Murciano A, Meseguer-Olmo L, De Aza PN. Assessment of Effects of Si-Ca-P Biphasic Ceramic on the Osteogenic Differentiation of a Population of Multipotent Adult Human Stem Cells. Materials. 2016; 9(12):969.
28. Jung GY, Park YJ, Han JS. Effects of HA released calcium ion on osteoblast differentiation. Journal of Materials Science: Materials in Medicine. 2010; 21(5):1649–1654. [PubMed: 20162336]
29. Kim HL, Jung GY, Yoon JH, Han JS, Park YJ, Kim DG, Zhang M, Kim DJ. Preparation and characterization of nano-sized hydroxyapatite/alginate/chitosan composite scaffolds for bone tissue engineering. Materials Science and Engineering: C. 2015; 54:20–25. [PubMed: 26046263]
30. Young TJ, Monclus MA, Burnett TL, Broughton WR, Ogin SL, Smith PA. The use of the PeakForce TM quantitative nanomechanical mapping AFM-based method for high-resolution Young's modulus measurement of polymers. Measurement Science and Technology. 2011; 22(12): 125703.
31. Loh QL, Choong C. Three-Dimensional Scaffolds for Tissue Engineering Applications: Role of Porosity and Pore Size, Tissue Engineering. Part B, Reviews. 2013; 19(6):485–502.
32. Dan Y, Liu O, Liu Y, Zhang Y-Y, Li S, Feng X-b, Shao Z-w, Yang C, Yang S-H, Hong J-b. Development of Novel Biocomposite Scaffold of Chitosan-Gelatin/Nanohydroxyapatite for Potential Bone Tissue Engineering Applications. Nanoscale Research Letters. 2016; 11:487. [PubMed: 27822909]
33. Jian YT, Yang Y, Tian T, Stanford C, Zhang XP, Zhao K. Correction: Effect of Pore Size and Porosity on the Biomechanical Properties and Cytocompatibility of Porous NiTi Alloys. PLOS ONE. 2016; 11(2):e0149051. [PubMed: 26848842]
34. Poralan JGM, Gambe JE, Alcantara EM, Vequizo RM. X-ray diffraction and infrared spectroscopy analyses on the crystallinity of engineered biological hydroxyapatite for medical application. IOP Conference Series: Materials Science and Engineering. 2015; 79(1):012028.
35. Xu X, Wang X. Fine tuning of the sizes and phases of ZrO2 nanocrystals. Nano Research. 2009; 2(11):891.
36. Sekhar P, Padma Kumar H, Pazhani R, Solomon S, Thomas J. Synthesis, characterization and microwave dielectric properties of nanocrystalline CaZrO3 ceramics. 2008
37. Iviglia G, Cassinelli C, Torre E, Baino F, Morra M, Vitale-Brovarone C. Novel bioceramic-reinforced hydrogel for alveolar bone regeneration. Acta Biomaterialia. 2016; 44:97–109. [PubMed: 27521494]

38. Zhu Y, Dong Z, Wejinya UC, Jin S, Ye K. Determination of mechanical properties of soft tissue scaffolds by atomic force microscopy nanoindentation. J Biomech. 2011; 44(13):2356–61. [PubMed: 21794867]

39. Song YG, Cho IH. Characteristics and osteogenic effect of zirconia porous scaffold coated with β-TCP/HA. The Journal of Advanced Prosthodontics. 2014; 6(4):285–294. [PubMed: 25177472]

Highlights

- Similarity in compressive property of porous CS-nHA to CS-nZrO and CS-nCZ composite scaffolds.
- Comparable nano-mechanical property of CS-nHA, CS-nZrO, and CS-nCZ composite materials.
- Higher cell proliferation on CS-nHA and CS-nCZ compared to CS and CS-nZrO.
- CS-nHA and CS-nCZ can behave similarly to promote cells proliferation and spreading.

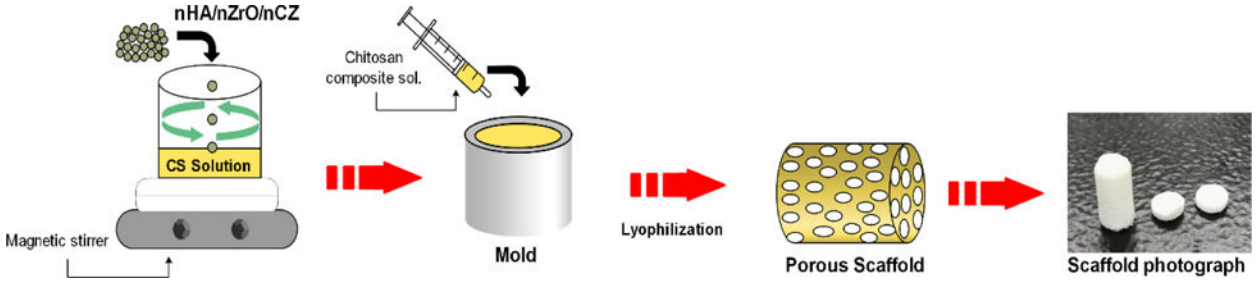

Figure 1.
Schematic representation of scaffold fabrication process.

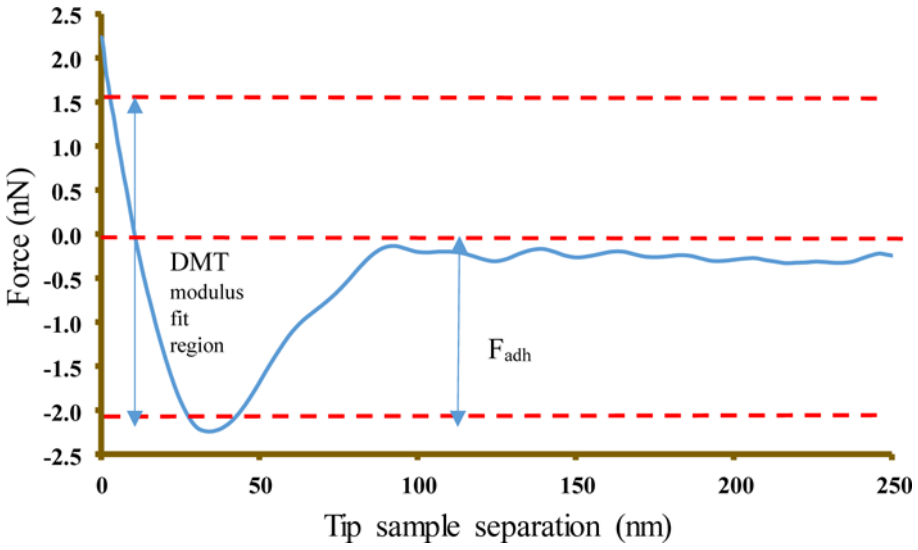

Figure 2.
Force-separation curve obtained after nanomechanical mapping by AFM.

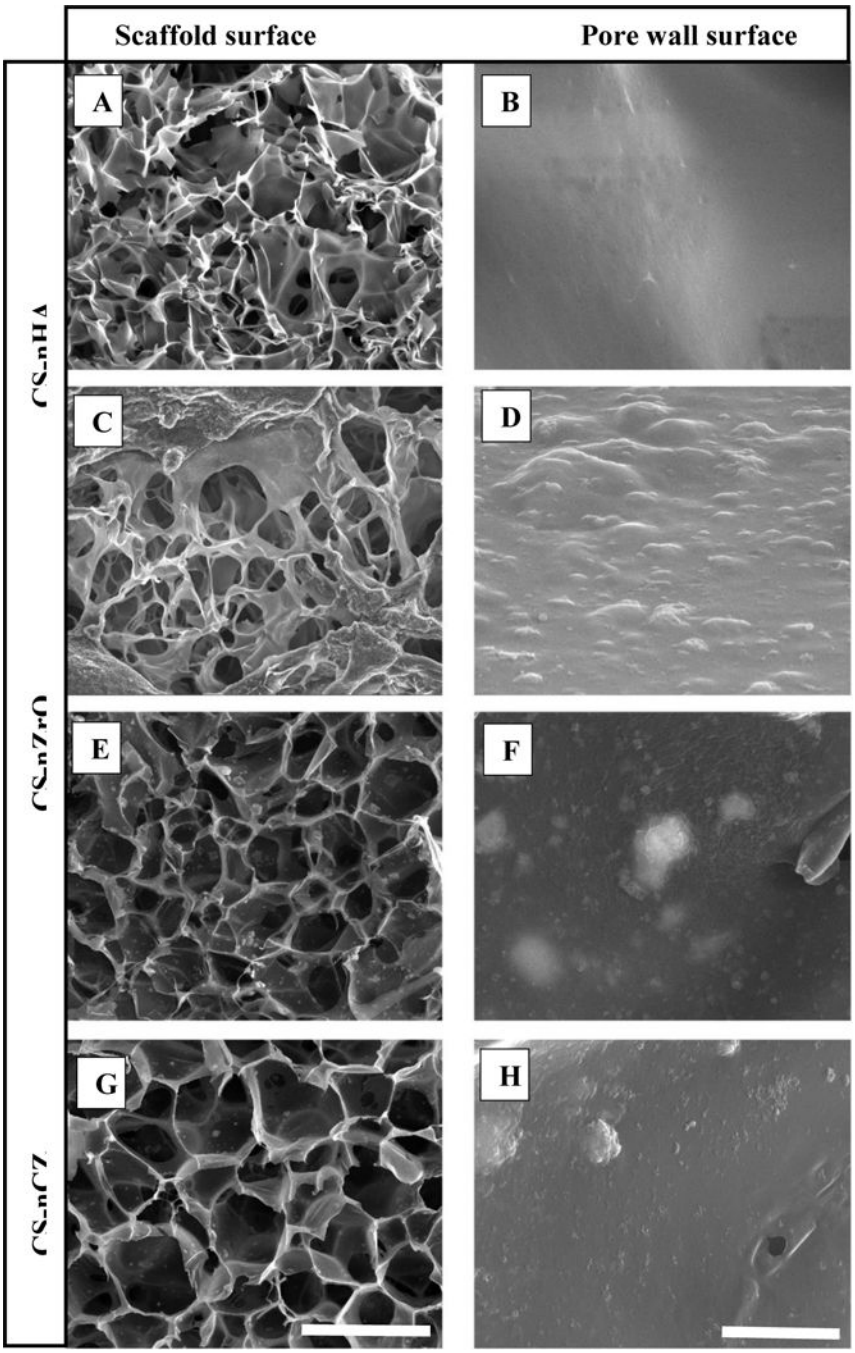

Figure 3.
SEM images showing the highly porous morphology of scaffold surface (A, C, E, and G) and magnified image showing the surface of scaffold wall (B, D, F, and H). (Scale: 100 μm for scaffold surface and 2 μm for pore wall surface).

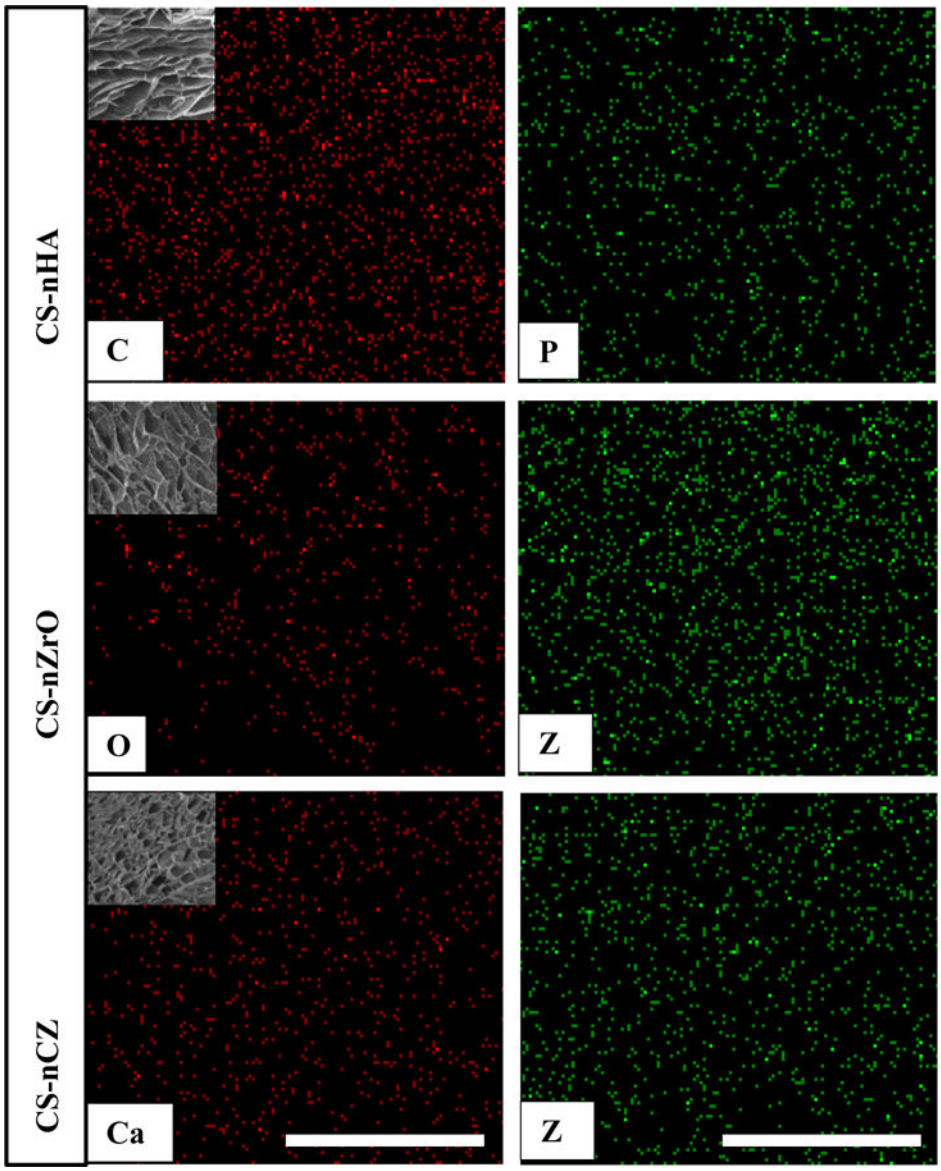

Figure 4.
Elemental map of composite scaffolds using EDS done to observe the distribution of nanoparticles along their surface. (Scale: 300 μm) (Ca: calcium, P: phosphorous, O: oxygen, Zr: zirconium).

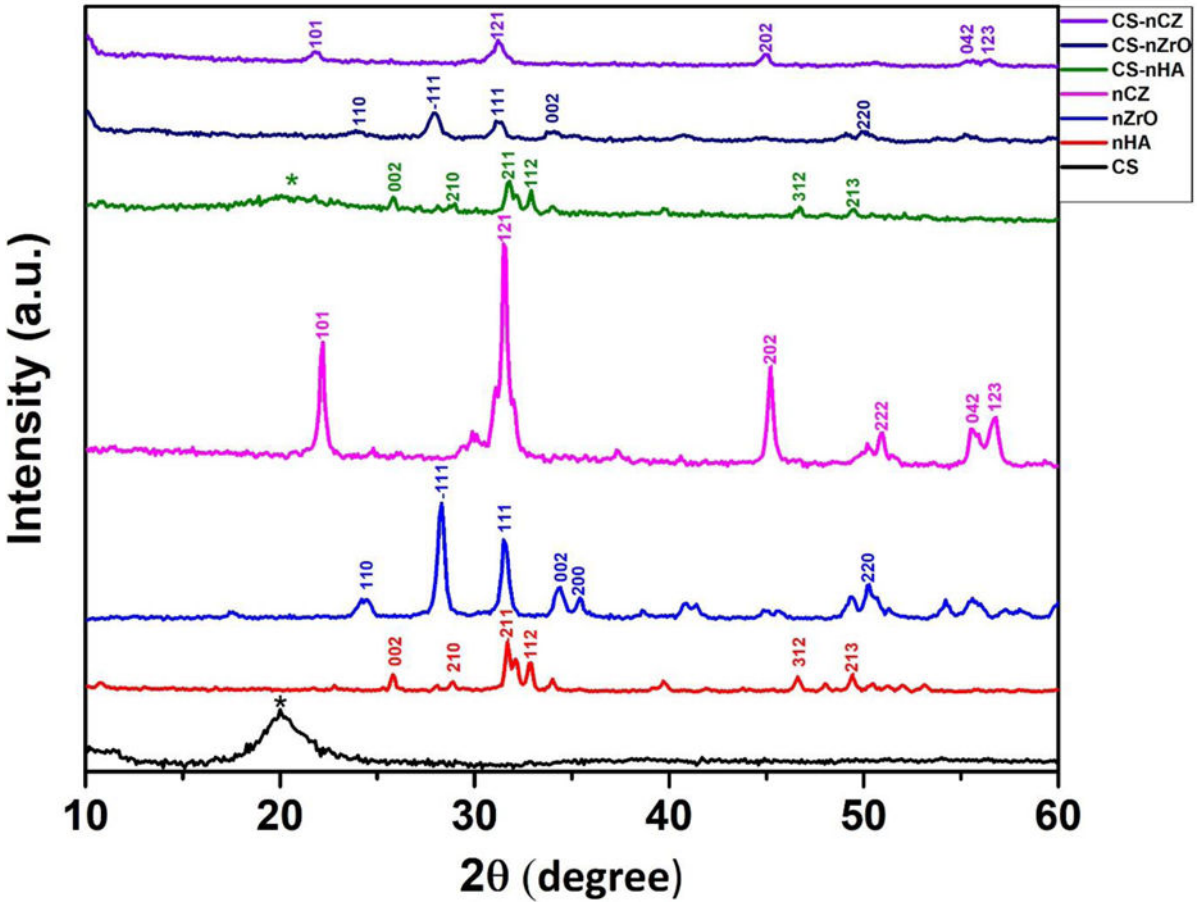

Figure 5.
XRD pattern of bulk material powder and composite scaffolds. * represents CS peak)

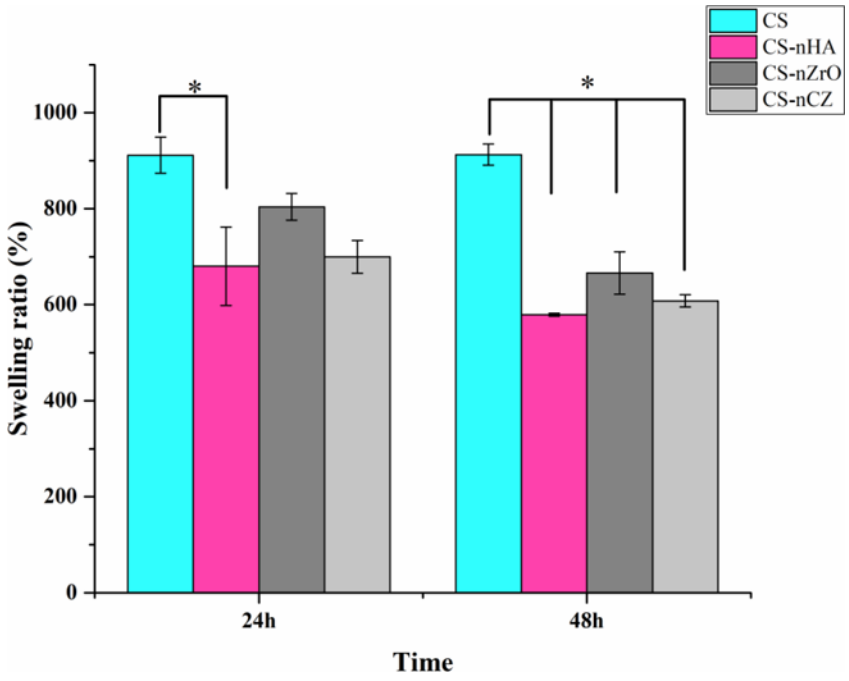

Figure 6.

Water absorption capacity of different scaffolds after 24 h and 48 h. CS only scaffolds absorbed more water and thus swelled more than composite scaffolds. * represents the significant between groups indicated ($p<0.05$).

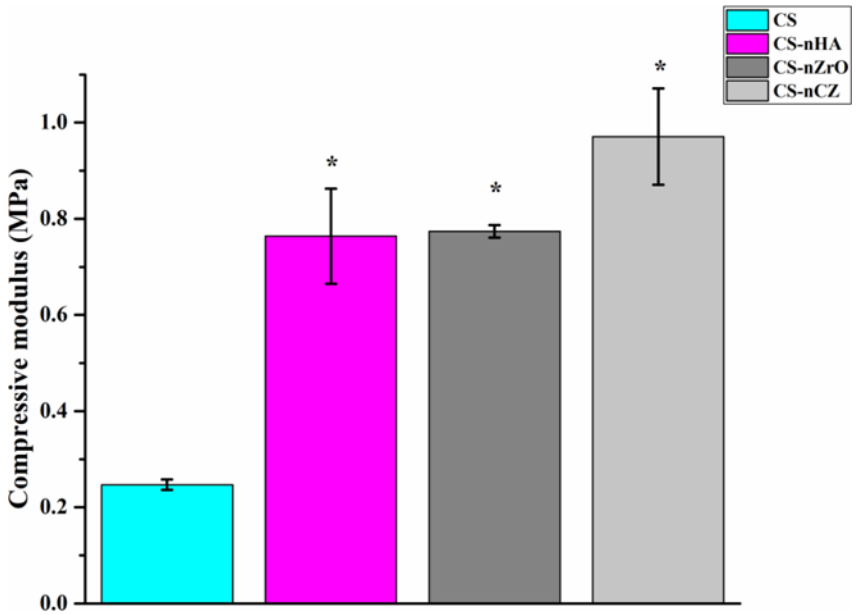

Figure 7.

Compressive strength and modulus of scaffolds. Compressive property was improved significantly on all CS-composite scaffolds compared to CS only scaffolds. * represents the significant difference than the CS-group.

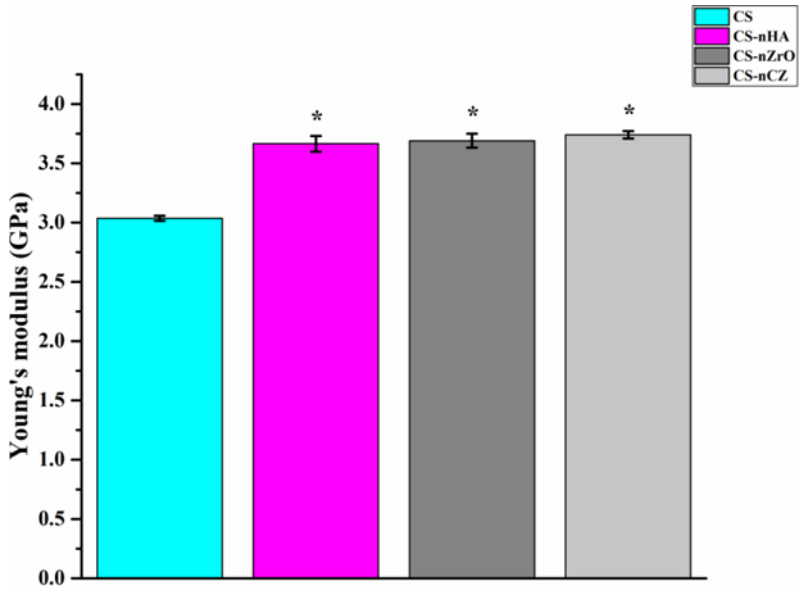

Figure 8.

Nano-mechanical property of scaffold materials determined using AFM in PFQNM. All composite groups had higher Young's modulus compared to CS only scaffolds. * represents the significant difference than CS group.

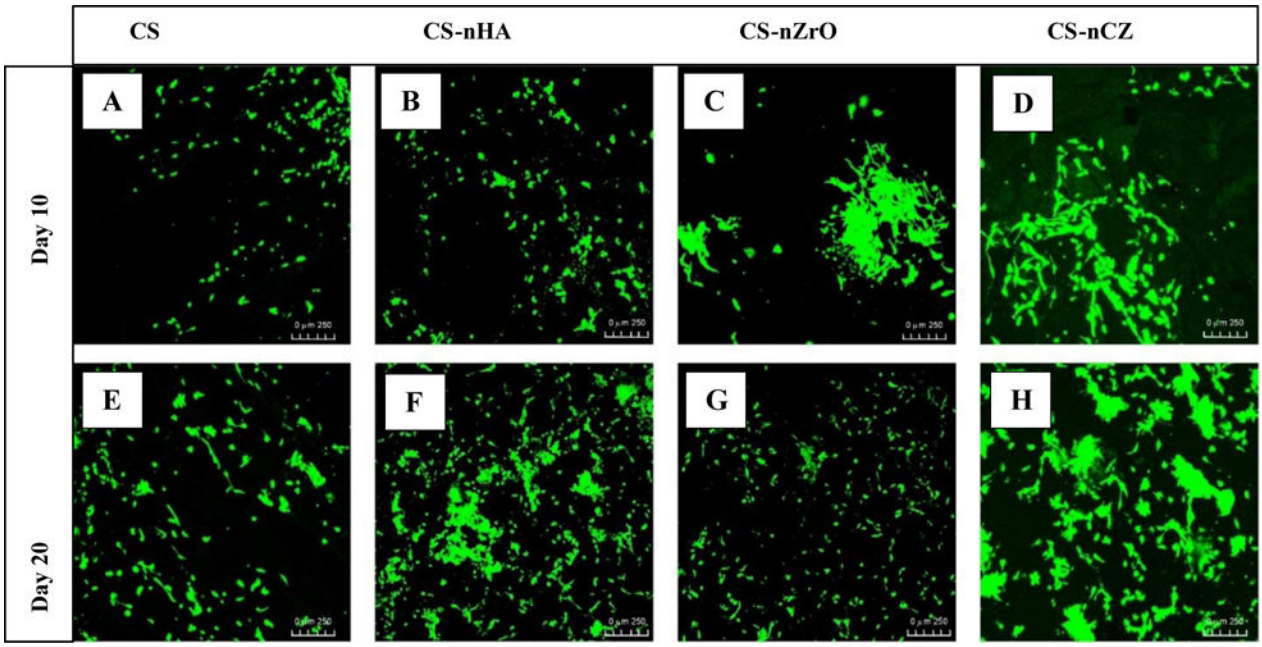

Figure 9.

Proliferation of OB-6 pre-osteoblasts on CS and CS composite scaffolds at day 10 and 20. The proliferation was better on CS-nHA and CS-nCZ groups. (Scale: 250 μm)

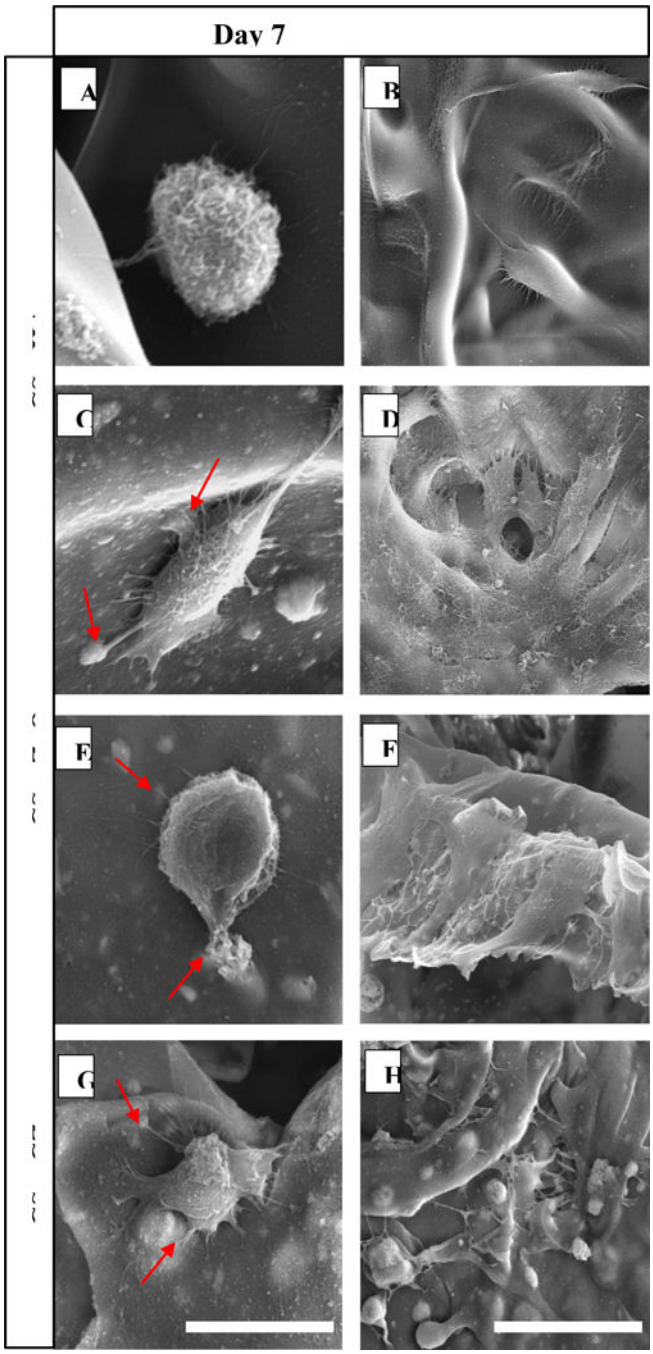

Figure 10.
SEM images showing the morphology of pre-osteoblast attached and proliferating along the surface of different scaffolds. (Scale: 20 μm for day 7 and 50 μm for day 14 images).